JOURNAL OF MATERIALS SCIENCE 13 (1978) 1717–1724

An automatic system for X-ray diffraction line profile analysis

F. RAITERI, A. SENIN
Laboratori di Ricerca, Ing. C. Olivetti S. p. A., Ivrea, Italy

G. FAGHERAZZI
Istituto di Chimica Fisica dell'Università, Ca' Foscari D. D. 2137, Venezia, Italy

An automatic procedure for X-ray line profile Fourier analysis is described. The Fourier coefficients were computed by the Stokes method and the real parts were used as input data to the Warren–Averbach method, which separates the line broadening due to particle size from that due to microstrains and/or to stacking faults. With the present system all calculations and plots are performed by an appropriately coded minicomputer on-line interfaced with a linear X-ray diffractometer. This system was tested in two different applications. Cu filings (cold-worked) that give two first and second-order diffraction lines, and CdS thin films, prepared by sputtering, which give a single measurable reflection. In this case the Warren–Averbach method was partly modified. The particle size, microstrains and stacking fault probabilities were determined and the results are discussed.

1. Introduction

The present paper describes an automatic procedure for X-ray line profile Fourier analysis. The Fourier coefficients were computed by the Stokes method [1]. The real parts were used as input data to the Warren–Averbach method [2, 3]. This method was partly modified to deal with strongly oriented and/or poorly crystallized samples giving one measurable peak only [4, 5].

It is known that whenever two or more diffraction peaks of the same $h\,k\,l$ plane set are present, particle size and lattice disorder effects can be separated. From several review papers it appears that diffraction intensity data can be transferred to a computer and processed off-line. Moreover, at certain steps, graphs are needed to evaluate results. To our knowledge the R. J. de-Angelis and C. P. Gazzara computer programs are the most complete ones published at this time [6, 7]. With the present system, all the calculations are carried out by an appropriately coded Olivetti P 6060. The minicomputer is interfaced both to the step motor and to the timer-scaler of the X-ray powder diffractometer. The computer routine includes the following steps:

(a) Lorentz and polarization factors (optional)

(b) Background subtraction

(c) Rachinger $K\alpha_1 - \alpha_2$ doublet separation and peak baricentre determination [8].

(d) Stokes correction and calculation of the real Fourier coefficients $A(L)$ of the de-smeared line profile.

(e) Plot of $\ln A(L)$ versus h_0^2, where h_0^2 is equal to $(h^2 + k^2 + l^2)$ in the case of cubic lattices, and h, k, l are Laue indices of the line under examination. Plot of $A^{PF}(L)$ versus L, pertinent to particle size and fault broadening effects.

(f) Calculation of the r.m.s. microstrain as $\langle \epsilon_L^2 \rangle^{1/2}$ as function of the depth L (Å) in the real space.

The coherent diffracting domain size and stacking fault probabilities cannot be computed automatically due to the presence of the so-called "hook effect" [9]. However, these figures may be easily computed using parameters obtained from the $A^{PF}(L)$ versus L plots.

This system has been thoroughly tested in two different applications: Cu filings (cold-worked) that give two first and second-order diffraction lines, and CdS thin films, prepared by sputtering, which very often are strongly oriented and give a single measurable line. The results obtained in the

first case agree well with the values previously reported by other workers. A test on the same samples was carried out by comparing results obtained by the present method with those obtained by means of a non-automatic traditional processing of experimental data, in which graphs are used from the very beginning.

2. Theory

If $h_{\bar{\alpha}}(2\theta)$ is a measured peak profile, the $K\alpha_1$ line is resolved by applying the Rachinger relation:

$$h_{\bar{\alpha}}(2\theta) = h_{\alpha_1}(2\theta) + 1/2\, h_{\alpha_1}(2\theta - \Delta 2\theta_{\alpha_1-\alpha_2}) \tag{1}$$

where $\Delta 2\theta_{\alpha_1-\alpha_2}$ is the angular doublet separation and 2θ is the Bragg angle. The $h_{\alpha_1}(2\theta)$ or $h_{\alpha_1}(s)$ peak, where s is equal to $2\sin\theta/\lambda$ and λ is the wavelength of the radiation, is broadened by instrumental factors. The instrument function is taken into account by considering the $g_{\alpha_1}(s)$ peak, produced by a well-annealed sample. The true line profile, $f_{\alpha_1}(s)$, is given, according to Stokes, by

$$h_{\bar{\alpha}_1}(s) = \int_{-\infty}^{+\infty} f^*_{\alpha_1}(s)\, g_{\alpha_1}(s - s^*)\, \mathrm{d}s^* \tag{2}$$

Stokes has shown that the Fourier coefficients $F(L)$ of the true line profile are given by

$$F(L) \equiv A(L) + \mathrm{i}B(L) = \frac{H(L)}{G(L)} \tag{3}$$

where $H(L)$ and $G(L)$ are the Fourier coefficients of the $h_{\alpha_1}(s)$ and $g_{\alpha_1}(s)$ respectively. In this way $f_{\alpha_1}(s)$ is given by:

$$f_{\alpha_1}(s) = \sum_{-\infty}^{+\infty} [A(L)\cos 2\pi L(s - s_0) + B(L)\sin 2\pi L(s - s_0)] \tag{4}$$

If the baricentre s_0 of the peak is chosen as origin of the Fourier analysis, and the line is nearly symmetrical, the real coefficients $A(L)$ are nearly equal to $|F(L)|$ and $B(L)$ are nearly zero.

Warren and Averbach have shown that for small L values, each $A(L)$ coefficient can be expressed as:

$$A(L) = A^{PF}(L) \cdot A^{\epsilon}(L) \tag{5}$$

where $A^{PF}(L)$ depends on particle size and faults and $A^{\epsilon}(L)$ depends on microstrains. For $A^{PF}(L)$ and $A^{\epsilon}(L)$ we have the following relationships for small L values and cubic lattices:

$$A^{PF}(L) = 1 - \frac{1}{D_{eff}(hkl)} \tag{6}$$

$$A^{\epsilon}(L) = 1 - \frac{2\pi^2 L^2 \langle \epsilon^2 \rangle_{hkl} h_0^2}{a^2} \approx \exp \frac{-2\pi^2 L^2 \langle \epsilon_L^2 \rangle_{hkl} h_0^2}{a^2} \tag{7}$$

where a is the lattice parameter, $D_{eff}(hkl)$ is the effective crystallite size along the direction perpendicular to the (hkl) planes, $\langle \epsilon_L^2 \rangle_{hkl}$ is the average "microstrain" along the $[hkl]$ direction.

Equation 7 is not only valid for cubic lattices, in which case a is the unit cell edge and $h_0^2 = h^2 + k^2 + l^2$, but also, for example, for $00l$ reflections of hexagonal lattices, in which case $h_0 = l$ and $a = d_{001}$; $1/D_{eff}(hkl)$ can also be written as:

$$\frac{1}{D_{eff}(hkl)} = \frac{1}{\bar{D}(hkl)} + \frac{(1.5\alpha + \beta)V_{hkl}}{a} \tag{8}$$

where $\bar{D}(hkl)$ is the "true" average length of the diffracting coherent domains along the $[hkl]$ direction, α and β are two different probabilities of faults (α = deformation, β = twin faults). V_{hkl} are coefficients that for f c c lattices are defined by:

$$V_{hkl} = \sum_b \frac{|L_0|}{h_0(u + b)} \tag{9}$$

where $L_0 = h + k + l$; b is the number of reflection components affected by stacking faults ($L_0 = 3N \pm 1$ with N integral) and u is the number of the reflection components not affected by stacking faults ($L_0 = 3N$). As can be seen from Equations 6, 7 and 8, the coefficients $A(L)$ depend on the diffraction order h_0. The separation of particle size broadening from other broadening effects is based on this. Substituting from Equation 6 and 7 into Equation 5, the following relation is obtained:

$$\ln A(L) = \ln A^{PF}(L) - 2\pi^2 L^2 \langle \epsilon_L^2 \rangle \cdot \frac{h_0^2}{a^2} \tag{10}$$

From the plot of $\ln A(L)$ versus h_0^2 for different L values, it is possible to obtain $\ln A(L)$ at $h_0^2 = 0$, i.e. the $A^{PF}(L)$ coefficients.

From the slope of the curve $A^{PF}(L)$ versus L, we obtain the effective average diameters:

$$-\left(\frac{\mathrm{d}A^{PF}(L)}{\mathrm{d}L}\right)_{L=0} = \frac{1}{D_{eff}(hkl)} \tag{11}$$

From the V_{hkl} values given by Equation 9 it is

easy to see that the contribution of stacking faults to $1/D_{\mathrm{eff}}(h\,k\,l)$ is $4/\sqrt{3} = 2.31$ times greater for the reflection (2 0 0) than for the reflection (1 1 1).

All the forementioned theory is based on the presence of at least two lines of the same $h\,k\,l$ set. To apply Equation 10 we need at least two h_0^2 values. When one line only is present, Charlson *et al.* [4] have shown that for small L values, the following expression can be used:

$$A(L) = 1 - \frac{L}{D_{\mathrm{eff}}} - C^2\langle\epsilon_L^2\rangle L^2 + \frac{C^2\langle\epsilon_L^2\rangle L^3}{D_{\mathrm{eff}}} \tag{12}$$

where

$$C^2 = \frac{2\pi^2 h_0^2}{a^2}$$

This expression can be deduced by substituting Equations 6 and 7 into Equation 5. By means of a third order least squares fit, D_{eff} and $\langle\epsilon_L^2\rangle$ can be determined separately.

In order to avoid the "hook" effect, we have used only the coefficients defined by L values between $0.1 \times D_{\mathrm{eff}}(\mathrm{min})$ and $D_{\mathrm{eff}}(\mathrm{min})$, where $D_{\mathrm{eff}}(\mathrm{min})$ is derived from the $A(L)$ versus L plots:

$$-\left(\frac{\mathrm{d}A(L)}{\mathrm{d}L}\right)_{L=0} = \frac{1}{D_{\mathrm{eff}}(\mathrm{min})}$$

In this way we do not take into account the micro-strain effects, and therefore the calculated parameters have to be considered as the minimum effective crystallite sizes. Another important point

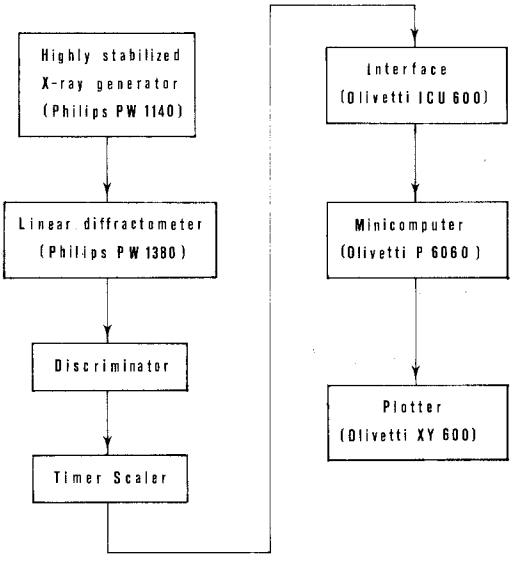

Figure 1 Hardware scheme employed.

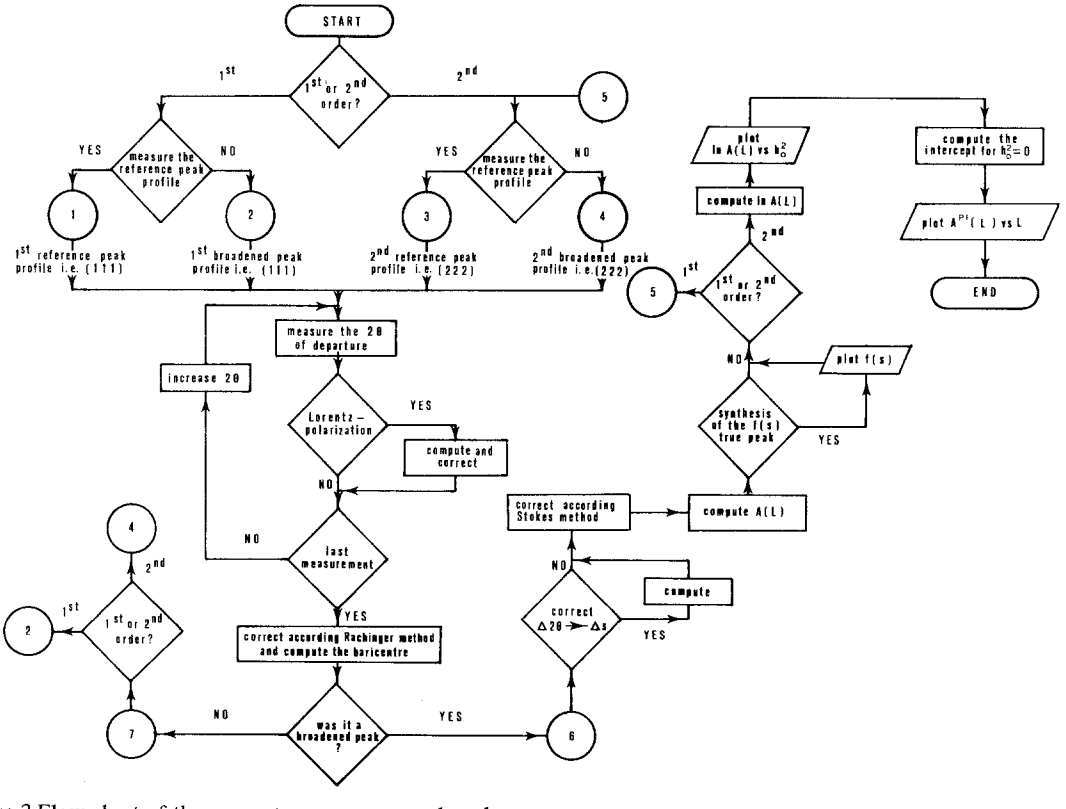

Figure 2 Flow-chart of the computer programs employed.

in this single peak analysis is that stacking faults (when present) cannot be separated from crystallite size broadening effects. Therefore only the "effective" and not the true crystallite size can be determined.

Equation 5 can be written as:

$$A^{PF}(L) = A(L) \exp\{C^2 \langle \epsilon_L^2 \rangle L^2\} \quad (13)$$

This is going back to the Warren–Averbach method; the D_{eff} value computed from the reciprocal of the slope of the curve $A^{PF}(L)$ versus L, for small L values, should be in close agreement with the value computed by least squares fit. This method gives the best results only when L values are allowed to vary slightly to reach the best agreement with the D_{eff} computed from the $A(L)$ versus L curve. L limits must be inside the previously defined interval.

3. Data collection and processing

A Philips powder diffractometer equipped with Soller slits, pulse height discrimination and solid state scintillation counter was used with Ni-filtered CuKα radiation. Intensities were automatically collected by step-scanning and fixed counts techniques. Standard conditions were 40 000 counts and a step of 0.02°. At $\theta \leqslant 60°$ this is equivalent to working with $\Delta 2\theta$ = constant. However, provision was made to convert data from $\Delta 2\theta$ to Δs = constant by means of a short subroutine.

With the present hardware system the data processing is made more accurate and faster, taking into account dead time due to data transferring. New programs, linked in a chain mode, were written in "BASIC" for the Olivetti P6060 machine. The hardware scheme is shown in Fig. 1, while Fig. 2 shows the flow-chart of the whole program. At different steps it is possible to produce diagrams and graphs, aiding evaluation of the process. The single peak analysis was also performed automatically, inserting a suitable subroutine (least squares) according to the given theoretical outline.

Diagrams for comparison with the automatic method were recorded at $1/8° \, min^{-1}$. After background subtraction, intensities were deduced graphically. These data were transferred to a computer, coded with the already published programs.

4. Sample preparation

Cold-worked Cu was obtained by filing an electrolytically pure copper block, at both room temperature and liquid nitrogen temperature (−180° C). As a reference sample we used a Cu powder, annealed in a hydrogen atmosphere at 450° C for 8 h.

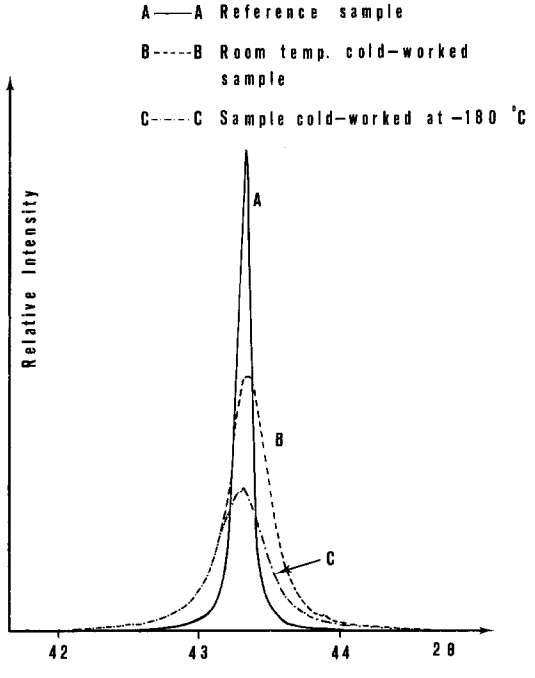

Figure 3 Relative intensity of the (1 1 1) K_{α_1} peak profile for the three Cu samples examined after Rachinger separation.

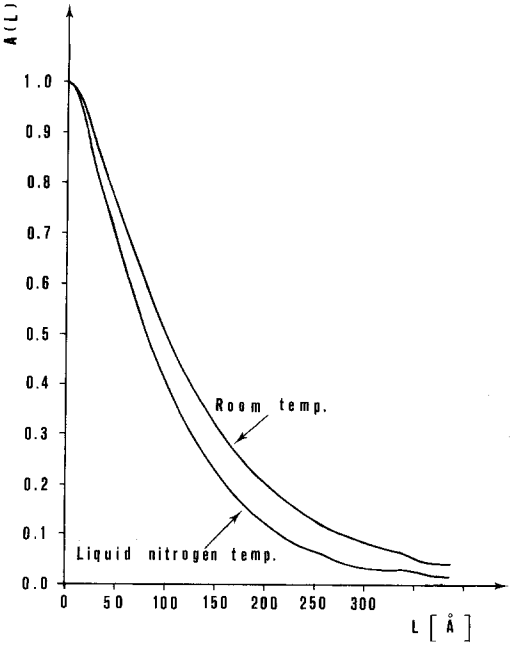

Figure 4 $A(L)$ versus L plot of the (1 1 1) peak for the cold-worked Cu samples.

TABLE I Effective particle sizes along the two crystallographic directions [1 1 1] and [1 0 0] for both Cu filings

Metal	Deformation temperature	Measurement temperature	$D_{eff}(1\,1\,1)$ (Å)	$D_{eff}(1\,0\,0)$ (Å)	$\frac{D_{eff}(1\,1\,1)}{D_{eff}(1\,0\,0)}$	$\frac{D_{eff}(1\,1\,1)}{D_{eff}(1\,0\,0)}$ (Ref)	Reference	$1.5\alpha + \beta$
Cu	Room	Room	170	85	2.00	2.00	[10]	0.044
Cu	− 180° C	Room	140	69	2.03	–		0.055

For all three powders, the fraction with particles sizes less than 40 μm was used. CdS thin films were deposited by sputtering on a glass substrate starting from a pre-sintered powder of reagent grade. One sample was annealed 1 h at 500° C in an inert atmosphere, in order to compare its microstructural properties with those of the non-treated thin film. A CdS powder of reagent grade was chosen as a reference sample with a large enough particle size. CdS crystallizes in the $P6_3mc$ space group with $a = 4.136$ Å and $c = 6.713$ Å.

5. Results and discussion

Fig. 3 shows three $K\alpha_1$ line profiles produced by the plotter, after Rachinger separation, for the (1 1 1) reflection. Curve A refers to the non-deformed reference Cu powder; B refers to the Cu, cold-worked at room temperature; and C refers to the Cu, cold-worked at liquid nitrogen temperature. The corresponding $A(L)$ versus L curves are shown in Fig. 4. Fig. 5 shows the non-normalized $\ln A(L)$ versus h_0^2 at different L values for the (1 1 1)–(2 2 2) lines, and for samples deformed at room temperature. Fig. 6 shows the $A^{PF}(L)$ versus L curve, deduced from the zero intercepts of the lines in Fig. 5. Two values of D_{eff} are shown here, 170 and 185 Å, the smaller being derived taking into account the hook effect. Analogous plots were derived for the (2 0 0)–(4 0 0) lines for both copper filings.

Table I summarizes the results obtained for the effective crystallite size $D_{eff}(h\,k\,l)$ in comparison with those reported by other authors. From the values of $D_{eff}(1\,1\,1)$ and $D_{eff}(1\,0\,0)$ the fault probabilities $(1.5\alpha + \beta)$ were deduced by applying Equation 8, taking $\bar{D}_{1\,1\,1} \cong \bar{D}_{1\,0\,0}$. The last colum of Table I gives these values. Table II summarizes the results obtained for the values $\langle \epsilon^2_{70\text{Å}} \rangle^{1/2}$ computed along the two directions [1 1 1] and [1 0 0]. In Table I it is worth noting that effective particle size decreases for both the crystallographic directions [1 1 1] and [1 0 0] as the cold working temperature decreases from room temperature to liquid nitrogen temperature. On the contrary, the ratio $D_{eff}(1\,1\,1)/D_{eff}(1\,0\,0)$ is nearly constant, very similar to published values and not too far from the already discussed limit value (2.31).

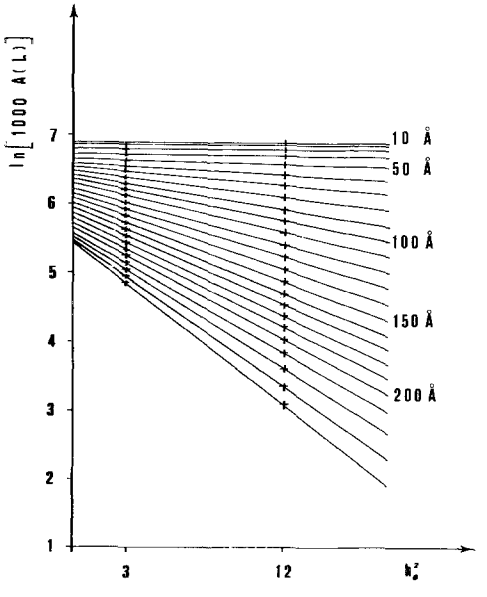

Figure 5 Ln [1000 $A(L)$] as a function of $h_0^2 = h^2 + k^2 + l^2$ for several L values. (1 1 1)–(2 2 2) peak couple. Cu sample cold-worked at room temperature. Plot obtained by automatic procedure.

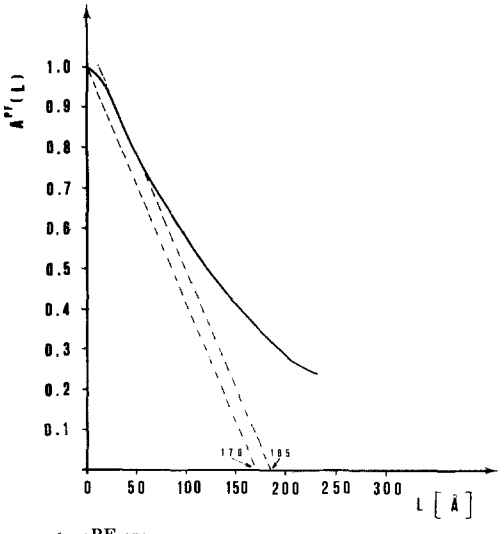

Figure 6 $A^{PF}(L)$ versus L plot for the (1 1 1)–(2 2 2) peak couple. Sample cold-worked at room temperature. The lowest value was obtained by taking into account the "hook" effect. Plot obtained by automatic procedure.

TABLE II R.m.s. microstrains measured on Cu filings applying the present automatic procedure and the Warren–Averbach method

Metal	Deformation temperature	Measurement temperature	$\langle\epsilon^2_{70}\text{Å}\rangle^{1/2}$ [1 1 1]	$\langle\epsilon^2_{70}\text{Å}\rangle^{1/2}$ [1 0 0]	$\langle\epsilon^2_{70}\text{Å}\rangle^{1/2}$ (Ref) [1 1 1]	$\langle\epsilon^2_{70}\text{Å}\rangle^{1/2}$ (Ref) [1 0 0]	Reference
Cu	Room	Room	0.0022	0.0016	0.0020	0.0029	[10]
Cu	−180° C	Room	0.0018	0.0017	–	–	–

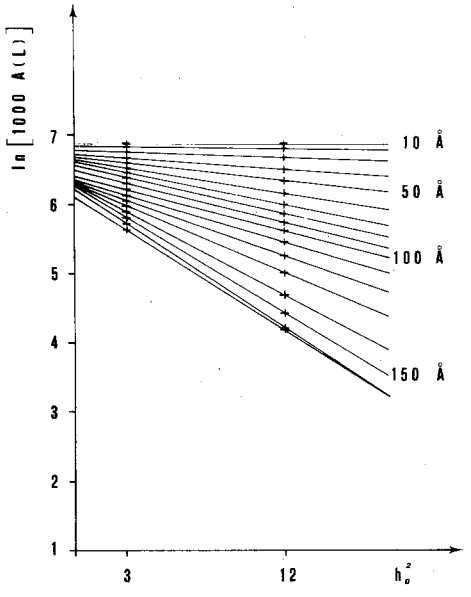

Figure 7 Ln [1000 $A(L)$] as a function of $h_0^2 = h^2 + k^2 + l^2$ for several L values. (1 1 1)–(2 2 2) peak couple. Cu sample cold-worked at room temperature. Plot obtained by graphical recording and off-line data computation.

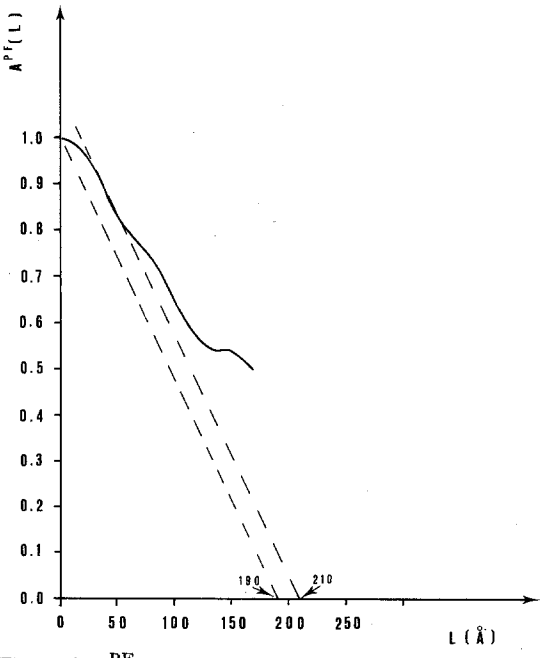

Figure 8 $A^{PF}(L)$ versus L plot for the (1 1 1)–(2 2 2) peak couple. Sample cold-worked at room temperature. The lowest value was obtained by taking into account the "hook" effect. Plot obtained by graphical recording and off-line data computation.

This result can be explained by the fact that, $\bar{D}_{1\,1\,1}$ and $\bar{D}_{1\,0\,0}$ being taken as equal, the observed anisotropy must be attributed mainly to the presence of stacking faults. It also explains the high values found for $(1.5\,\alpha + \beta)$.

Figs. 7 and 8 show the plots corresponding to those of Figs. 5 and 6, deduced from the same diffraction lines, but obtained graphically instead of from an automatic recording. In this case the $A(L)$ versus L curve has strong superimposed ripples, due to poor measuring accuracy, mainly on the tails of the line. Similar results were obtained for all observed peaks. It is worth noting that, due to the presence of the "hook effect", it is not possible to compute automatically the derivative present in Equation 11. Therefore we had to correct for this effect graphically, as shown in Figs. 6 and 8.

Fig. 9 shows the low-speed diffraction patterns of the three CdS samples. Due to preferred orientation in thin films patterns, the (1 0 0) and (1 0 1) lines disappear. The analysis of the (0 0 2) line profile, automatically stepped, has led to the results shown in Fig. 10, where the $A(L)$ versus L plots are shown for both CdS thin films. From these plots the minimum D_{eff} values have been derived, as shown in Figs. 10 and 11. These are in good agreement with those obtained by a least squares fit.

Fig. 11 shows $A^{PF}(L)$ versus L curves deduced from Equation 13, where we introduced the values of $\langle\epsilon_L^2\rangle$ computed via a least squares fit.

The D_{eff} particle diameters obtained from the $A^{PF}(L)$ versus L plots are given in the last column of Table III, while the D_{eff} values obtained by a least squares method are given in the third column. The agreement between the corresponding values is very good. The second column shows the minimum D_{eff} sizes computed without considering microstrain effects. The values of $\langle\epsilon_L^2\rangle$, averaged over L, are given in the fourth column of Table III. It is clear, from the data of Table III, that even a

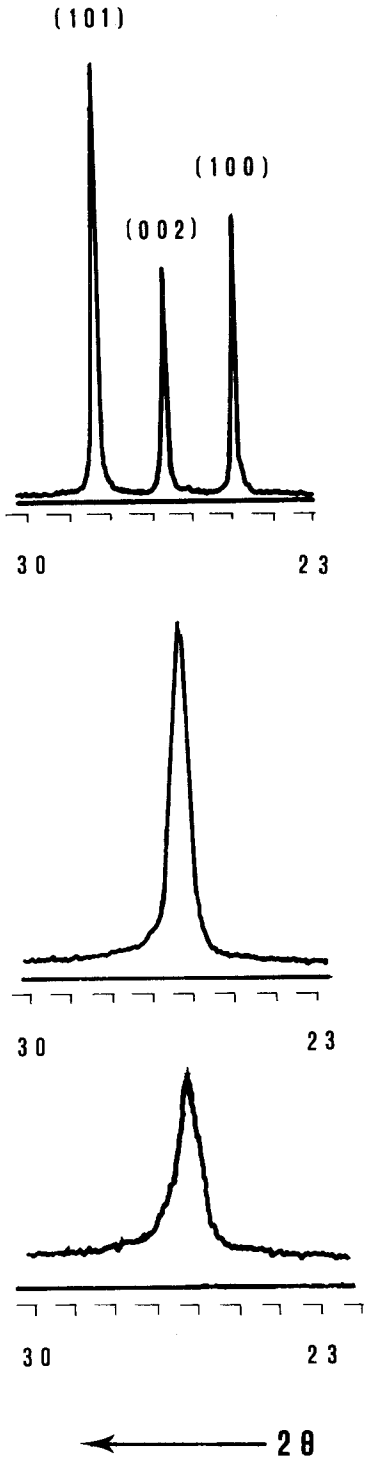

Figure 9 Low speed diffraction patterns of CdS samples. (A) Reference powder sample. (B) Thin film annealed at 500° C for 1 h. (C) Non-treated thin film.

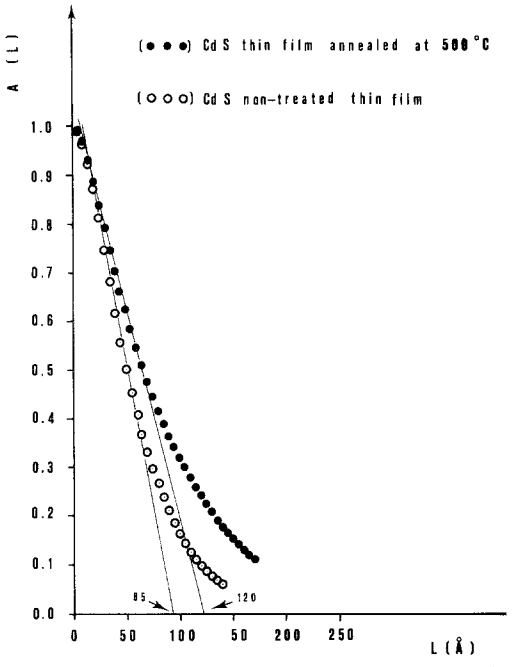

Figure 10 $A(L)$ versus L plots for both CdS thin films examined, from which the minimum D_{eff} values can be calculated, as shown.

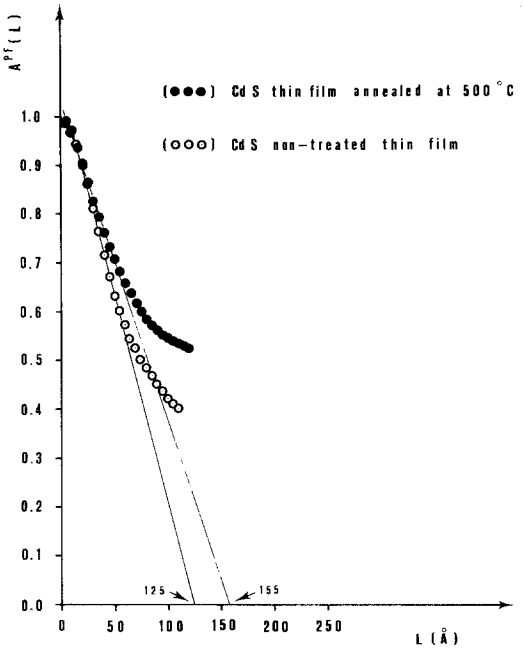

Figure 11 $A^{PF}(L)$ versus L plots for both CdS thin films examined, deduced from Equation 13, introducing $\langle \epsilon_L \rangle^2$ computed by a least squares method.

TABLE III Minimum effective particle sizes, effective particle sizes and microstrains for both the CdS thin films examined

Sample	D_{eff}(min); minimum value computed by W.A. method (Å)	D_{eff}; value computed by least squares method (Å)	$\langle \epsilon^2 \rangle^{1/2}$ computed by least squares method	Range used for the least squares fit (Å)	D_{eff} obtained from the $A^{PF}(L)$ versus L plot (Å)
CdS non-treated thin film	85	120	0.0073	5–85	125
CdS thin film annealed at 500° C for 1 h	120	145	0.0055	10–120	155

short annealing has greatly improved the crystallinity of the CdS thin film, both increasing the coherent diffraction domain sizes and decreasing the average microstrain value, which is proportional to the dislocations density.

References

1. A. R. STOKES, *Proc. Phys. Soc. (Lond.)* **B61** (1948) 382.
2. B. E. WARREN and B. L. AVERBACH, *J. Appl. Phys.* **21** (1950) 595.
3. *Idem, ibid.* **23** (1952) 497.
4. E. J. CHARLSON, DING HUA HU, M. R. FARUKHI, "Advances in X-ray Analysis", Vol. 14 (Plenum Press, New York, 1971) p. 441.
5. R. L. ROTHMAN and J. B. COHEN, "Advances in X-ray Analysis", Vol. 12 (Plenum Press, New York, 1969) p. 208.
6. R. H. de ANGELIS, "Local Atomic Arrangements Studied by X-ray Diffraction", (Gordon & Breach, New York, 1965) p. 271.
7. C. P. GAZZARA, J. J. STIGLICH Jr., F. P. MEYER and A. M. HANSEN, "Advances in X-ray Analysis", Vol. 12 (Plenum Press, New York, 1969) p.257.
8. W. A. RACHINGER, *J. Sci. Instrum.* **25** (1948) 254.
9. C. N. WAGNER, "Local Atomic Arrangements Studied by X-ray Diffraction", (Gordon & Breach, New York, 1965) p. 219.
10. D. E. MIKKOLA, J. B. COHEN, *ibid.* p. 289.

Received 12 July and accepted 14 November 1977.